

## Research Article

# Observations of an 11 September Sahelian Squall Line and Saharan Air Layer Outbreak during NAMMA-06

J. W. Smith,<sup>1,2</sup> A. E. Reynolds,<sup>2,3</sup> A. S. Pratt,<sup>4</sup> S. Salack,<sup>5</sup> B. Klotz,<sup>6</sup> T. L. Battle,<sup>1</sup> D. Grant,<sup>7</sup>  
A. Diop,<sup>5</sup> T. Fall,<sup>5</sup> A. Gaye,<sup>5</sup> D. Robertson,<sup>8</sup> M. S. DeLonge,<sup>9</sup> and S. Chan<sup>10</sup>

<sup>1</sup> Program in Atmospheric Sciences, Howard University, Washington, DC 20059, USA

<sup>2</sup> NASA Goddard Space Flight Center, Greenbelt, MD 20771, USA

<sup>3</sup> Atmospheric Science Group, Department of Geosciences, Texas Tech University, Lubbock, TX 79409, USA

<sup>4</sup> Earth Resources Technology, Inc., Laurel, MD 20707, USA

<sup>5</sup> Laboratory of Atmospheric Physics—Simeon Fongong, Cheikh Anta Diop University, Dakar, Senegal

<sup>6</sup> Rosenstiel School of Marine and Atmospheric Science, Cooperative Institute for Marine and Atmospheric Science Studies, University of Miami, Miami, FL 33149, USA

<sup>7</sup> Environmental Protection Agency, Region 4, Atlanta, GA 30303, USA

<sup>8</sup> Department of Mechanical Engineering, Howard University, Washington, DC 20059, USA

<sup>9</sup> Department of Environmental Science, Policy, and Management, University of California Berkeley, Berkeley, CA 94720, USA

<sup>10</sup> Department of Environmental Sciences, University of Virginia, Charlottesville, VA 22903, USA

Correspondence should be addressed to J. W. Smith, jonathan.smith@nasa.gov

Received 16 April 2011; Revised 28 September 2011; Accepted 5 November 2011

Academic Editor: Alessandra Giannini

Copyright © 2012 J. W. Smith et al. This is an open access article distributed under the Creative Commons Attribution License, which permits unrestricted use, distribution, and reproduction in any medium, provided the original work is properly cited.

The 2006 NASA-African Monsoon Multidisciplinary Analyses (NAMMA-06) field campaign examined a compact, low-level vortex embedded in the trough of an AEW between 9–12 September. The vortex triggered a squall line (SL) in southeastern Senegal in the early morning of 11 September and became Tropical Depression 8 on 12 September. During this period, there was a Saharan Air Layer (SAL) outbreak in northwestern Senegal and adjacent Atlantic Ocean waters in the proximity of the SL. Increases in aerosol optical thicknesses in Mbour, Senegal, high dewpoint depressions observed in the Kawsara and Dakar rawinsondes, and model back-trajectories suggest the SAL exists. The close proximity of this and SL suggests interaction through dust entrainment and precipitation invigoration.

## 1. Introduction

Westerly propagating squall lines (SLs) are frequent phenomena in the West African Sahel during the Northern Hemisphere summer [1, 2]. This SL formed and propagated ahead of the trough region of an African Easterly Wave (AEWs) [3, 4]. The development of SLs involves a combination of atmospheric conditions including conditional instability, low-level convergence, and vertical wind shear between relatively cool, moist, monsoon lower tropospheric air and warmer, drier Harmattan winds driven by the 650 hPa AEJ [3, 5].

The structure of SLs in West Africa was observed and analyzed during the Global Atmospheric Research Program's (GARP's) Atlantic Tropical Experiment (GATE) and

Convection Profonde Tropicale (COPT 81) field campaigns [3, 5–8]. Squall lines typically have a convective leading edge that produces a short period of intense rainfall. Observations show that intense precipitation extended 5 to 6 km above the surface (see reflectivity values of  $\geq 50$  dBZ in [7], Figure 8, [8], Figure 7). Observations and modeling studies suggest that SLs in the Sahel were embedded in the troughs of AEWs [3, 9, 10]. The axis of the AEW trough often contains two distinct mesoscale features: a low-level Saharan heat low to the north of the AEJ and a circulation at 650 to 700 hPa around 10°N [11–14]. The trough of the AEW highlighted as “Wave 7” of the 2006 NASA-African Monsoon Multidisciplinary Analyses (NAMMA-06) [15] took on these coupled dynamical features.

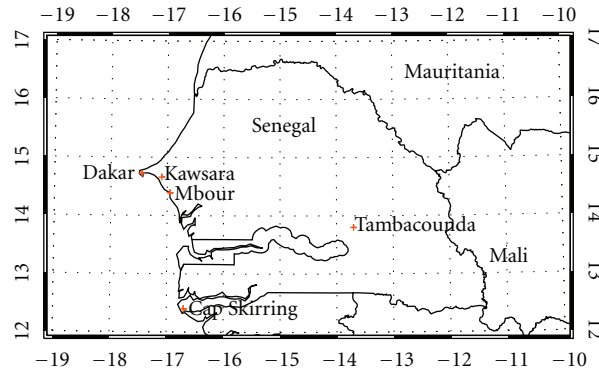


FIGURE 1: Map of cities and villages in Senegal where meteorological data relevant to this study was obtained.

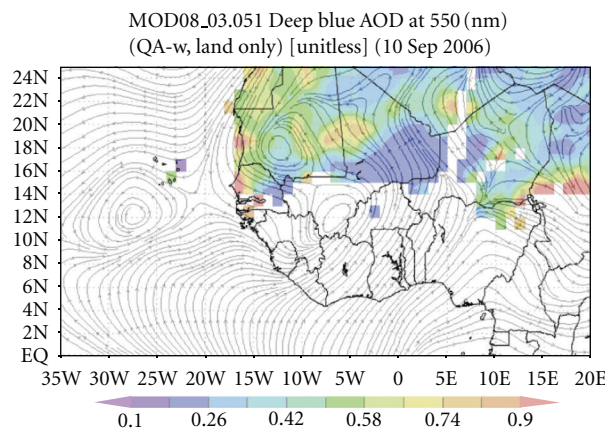


FIGURE 2: ECMWF Reanalyses streamlines and MODIS-Terra 550 nm AOT at 1200 UTC 10 September 2006.

The NAMMA-06 campaign extended from 15 August through 30 September 2006. The NAMMA-06 Campaign's goals were to find differences between AEWs that produce hurricanes and those that do not, the specific role of the Saharan Air Layer (SAL) has on AEWs and tropical cyclones, and to examine the role of cloud microphysics on precipitation amounts and contribution. The NAMMA-06 study accomplished the goals by observing seven AEWs and SAL outbreaks [15]. The SL in this study was one of two that developed with an AEW propagating westward out of Mali during the 9–11 September 2006 period and was a precursor to Hurricane Helene. Moreover, NAMMA-06 included an investigation of five SAL outbreaks and associated cloud microphysical properties [16].

The primary goals of this paper are to use data from the NAMMA-06 period to examine observations of an 11 September SL, SAL outbreak, and its interaction with the SL. Data locations and sources are discussed in Section 2 and the synoptic analysis and observations in Section 3. Observations of the 11 September SAL outbreak are presented in Section 4. A brief synthesis of the SL and SAL interaction is given in Section 5. Section 6 gives a summary of the major results and ideas for future work.

## 2. Data Locations and Sources

The locations of sites within Senegal where meteorological data were collected near the SL and SAL outbreak are presented in Figure 1. The European Center for Medium Range Weather Forecasting (ECMWF) 40-year (ERA-40) Reanalysis data are used to examine the synoptic-scale and mesoscale conditions in the vicinity of the SL. The ERA-40 Reanalysis covers the years of 1957–2010 and has a spatial and temporal resolution of approximately  $1^\circ \times 1^\circ$  and six hours, respectively [17]. The data and locations include flux tower measurements in Kawsara ( $14.7^\circ\text{N}$ ,  $17.1^\circ\text{W}$ ) (Figure 1), surface observations at the Cap Skirring Airport (GOGS) ( $12.4^\circ\text{N}$ ,  $16.7^\circ\text{W}$ ) (Figure 1), rawinsonde data from Kawsara, Leopold Sedar Senghor International Airport in Dakar (GOOY) ( $14.7^\circ\text{N}$ ,  $17.5^\circ\text{W}$ ), and Tambacounda Airport (GOTT) ( $13.8^\circ\text{N}$ ,  $13.7^\circ\text{W}$ ) (Figure 1). The National Centers for Environmental Prediction/Climate Prediction Center (NCEP/CPC) 4 km globally merged Infrared cloud top brightness temperature dataset [18] are used to evaluate the location and intensity of the SL convection. The merged IR product is also a Tropical Rainfall Measuring Mission (TRMM) ancillary dataset. Additional storm-scale data are

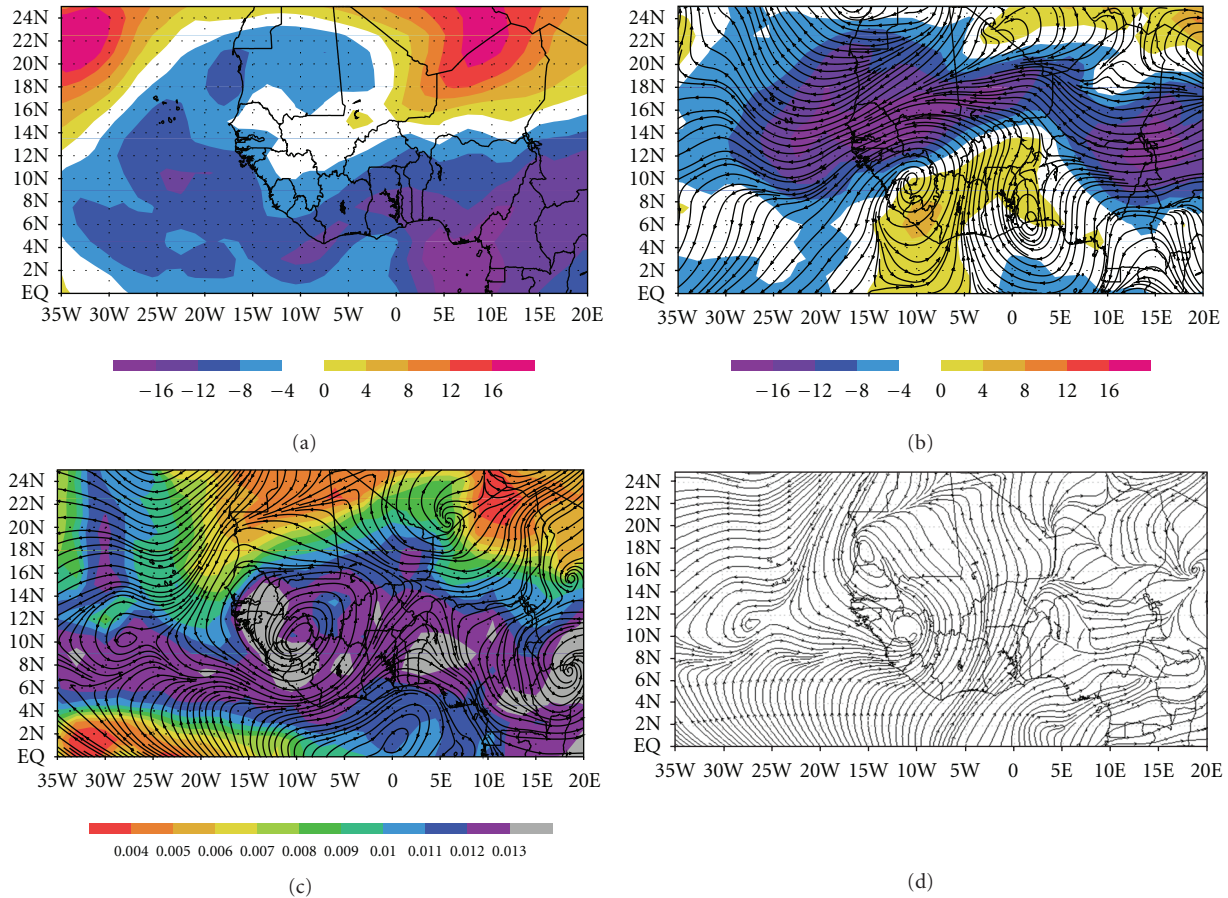


FIGURE 3: (a) ECMWF Reanalysis zonal winds ( $\text{m s}^{-1}$ ) at 0000 UTC 11 September for 200 hPa. (b) Composite ECMWF Reanalysis zonal winds ( $\text{m s}^{-1}$ ) and streamlines at 0000 UTC 11 September for 650 hPa. (c) Composite ECMWF Reanalysis specific humidity ( $\text{kg kg}^{-1}$ ) and streamlines at 0000 UTC 11 September for 850 hPa. (d) ECMWF Reanalysis streamlines at 0000 UTC 11 September for 925 hPa.

provided by the constant altitude plan position indicator (CAPPI) and radar height indicator (RHI) cross-sections from the NPOL radar (located in Kawsara), as well as the United Kingdom Meteorological Service Arrival Time Difference (UKMET ATD) cloud-to-ground lightning data set. The Aerosol Robotic Network (AERONET) Aerosol Optical Thickness (AOT) data from Mbour, Senegal ( $14.39^{\circ}\text{N}$ ,  $16.95^{\circ}\text{W}$ ), are used to indicate the presence of Saharan dust aerosols in the storm environment. Back-trajectories from the Hybrid Single Particle Lagrangian Integration Trajectory (HYSPLIT) Model and MODIS Terra satellite images over West Africa and the adjacent eastern Atlantic Ocean are examined to highlight the interaction between the SL and the SAL. Taken together, these data provide a robust and detailed picture of the environmental conditions for this case.

### 3. Squall Line Environmental Characteristics

**3.1. Synoptic View.** The 10 September 2006 MODIS-Terra 550 nm AOT (Figure 2) displays AOT values that exceed 0.9 in western Senegal. These values stretch northward into Mauritania. The 925 hPa flow from around a heat low in Southern Mauritania at 1200 UTC 10 September suggests

that air from dust aerosols in the Sahara are advecting into Senegal as early as 18 hours before the SL arrives.

The 0000 UTC analysis on 11 September 2006 depicts several large-scale dynamical features over West Africa. The Tropical Easterly Jet (TEJ) can be seen at 200 hPa extending from central Africa westward along the Gulf of Guinea coast, and then northwestward just offshore of Guinea-Bissau and Senegal (Figure 3(a)). This jet helped support upper-level divergence, which aided in repeated squall line development with this AEW.

A closed circulation exists within the AEW trough axis at 650 hPa, with the core of the AEJ just to its north (Figure 3(b)). This closed circulation is also noted at 850 hPa (Figure 3(c)) and 925 hPa (Figure 3(d)). A sharp gradient in specific humidity can be seen over Senegal at 850 hPa, separating the dry SAL regime from the much moister (specific humidity  $> 0.012 \text{ kg kg}^{-1}$ ) regime near the vicinity of the incipient squall line. A Saharan heat low is also present at 925 hPa (Figure 3(d)) over southern Mauritania; the flow around the heat low advects dust aerosols south and east toward central and eastern Senegal. This general circulation pattern is characteristic of some AEWs [11–14]. The same general circulation features were observed for this AEW with the Global Data Assimilation System analyses [15].



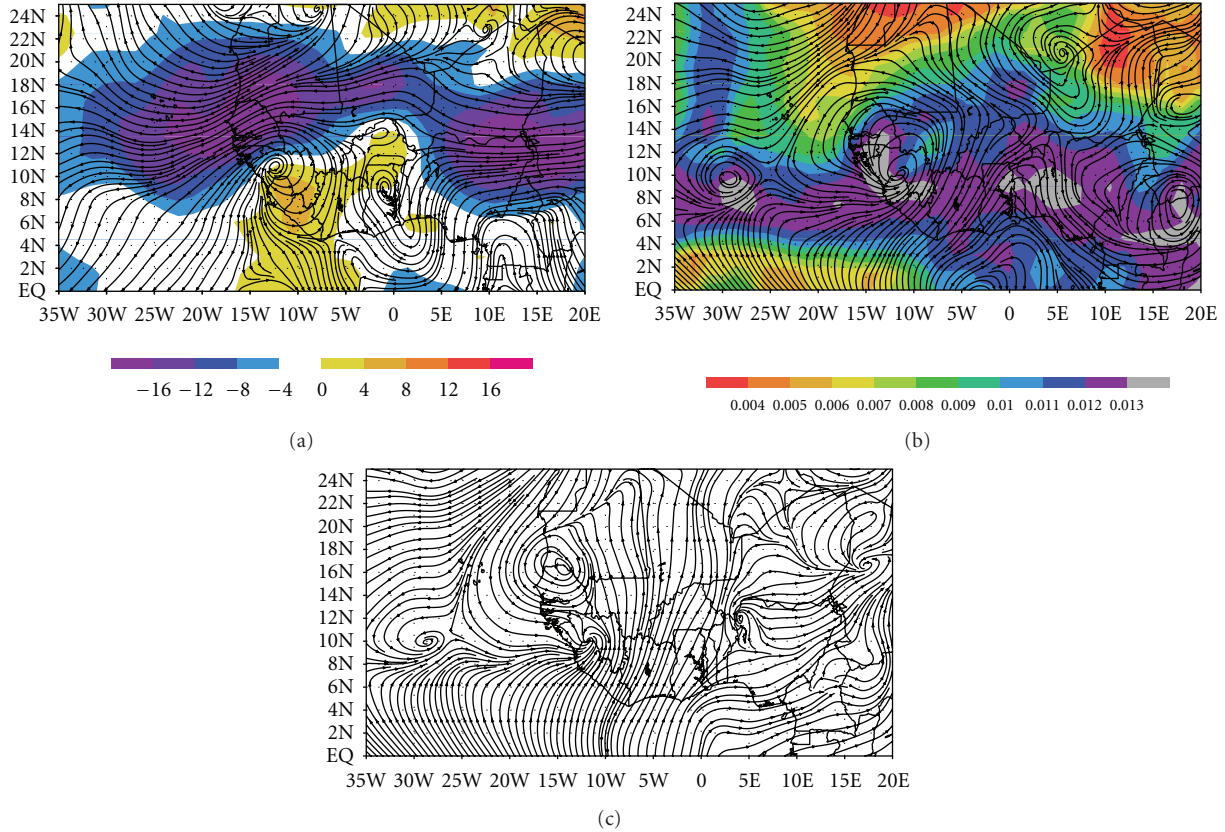


FIGURE 4: (a) Composite ECMWF Reanalysis zonal winds ( $\text{m s}^{-1}$ ) and streamlines at 0600 UTC 11 September for 650 hPa. (b) Composite ECMWF Reanalysis at 0600 UTC 11 September for 850 hPa, specific humidity ( $\text{kg kg}^{-1}$ ) and streamlines. (c) Composite ECMWF Reanalysis streamlines at 0600 UTC 11 September for 925 hPa.

At 0600 UTC (Figures 4(a)–4(c)), the low-level vortex associated with the AEW at 850 hPa and 925 hPa is located over southern Guinea ( $12^\circ\text{W}$ ,  $10^\circ\text{N}$ ). These features, along with the collocated 650 hPa AEW vortex and 925 hPa heat low over southern Mauritania, are propagating westward. The drier SAL regime has pushed further to the south (Figure 5(b)), while dust continues to be advected into the storm environment by the 925 hPa circulation. At 1200 UTC (Figure 5(a)–5(d)), the vortex at 850 hPa has moved further west with wind speeds increasing as suggested by the streamlines. The Saharan heat low (Figure 5(d)) moves southwestward to the northern coast of Senegal and the compact streamlines at 650 hPa suggest that the circulation is also strengthening. This circulation is centered 75–100 km east of the coast of Guinea and continues moving westward (Figure 5(b)). The position of these coupled features shows that the northern end of the AEW trough axis is moving faster than its southern end. Moreover, the 650 hPa circulation is located northwest of the 850 hPa circulation, indicating that the AEW circulation is tilted from southeast to northwest with height (Figure 5(c)).

**3.2. Satellite and Surface Observations.** The merged IR satellite observations (Figure 6) show the development and evolution of the convection associated with the AEW. This

particular AEW had a history of producing numerous squall lines; one such squall line can be seen moving offshore at 0000 UTC 11 September [15]. A second SL (the purpose of this study) is initiated in southeastern Senegal at 0200 UTC (Figure 6(b)). As this SL developed IR, its cloud-top temperatures cool to 200–220 K south of the  $14^\circ\text{N}$  latitude line (Figures 6(c)–6(f)); there is also an expansion of the cloud canopy associated with this system. The cooling cloud top temperatures are indicative of the SL intensifying; the cloud tops are coolest at 0600 UTC (Figure 6(d)). This system moved offshore between 0900–1000 UTC.

Pregust front/SL conditions in Kawsara and Cap Skirring (Figure 7(a)) show a steady west ( $270^\circ$ ) to west-northwest ( $300^\circ$ ) wind at both locations throughout the morning, providing moist low-level onshore flow into the region. The wind speeds range from  $3.0$  to  $8.0 \text{ m s}^{-1}$ . Meanwhile, the SL continued to propagate westward into a thermodynamic regime conducive for the maintenance of strong convection. Convective Available Potential Energy (CAPE) value of  $3237 \text{ J kg}^{-1}$  at 0000 UTC is observed at Dakar and  $4443 \text{ J kg}^{-1}$  at 0549 UTC at Kawsara (Table 1). At both locations, the CAPE exceeds one of the highest COPT 81 values of  $2810 \text{ J kg}^{-1}$  [9].

There was a marked temperature drop from  $28.0^\circ\text{C}$  at 0900 to  $22.0^\circ\text{C}$  at 1100 UTC at Cap Skirring (Figure 7(a))



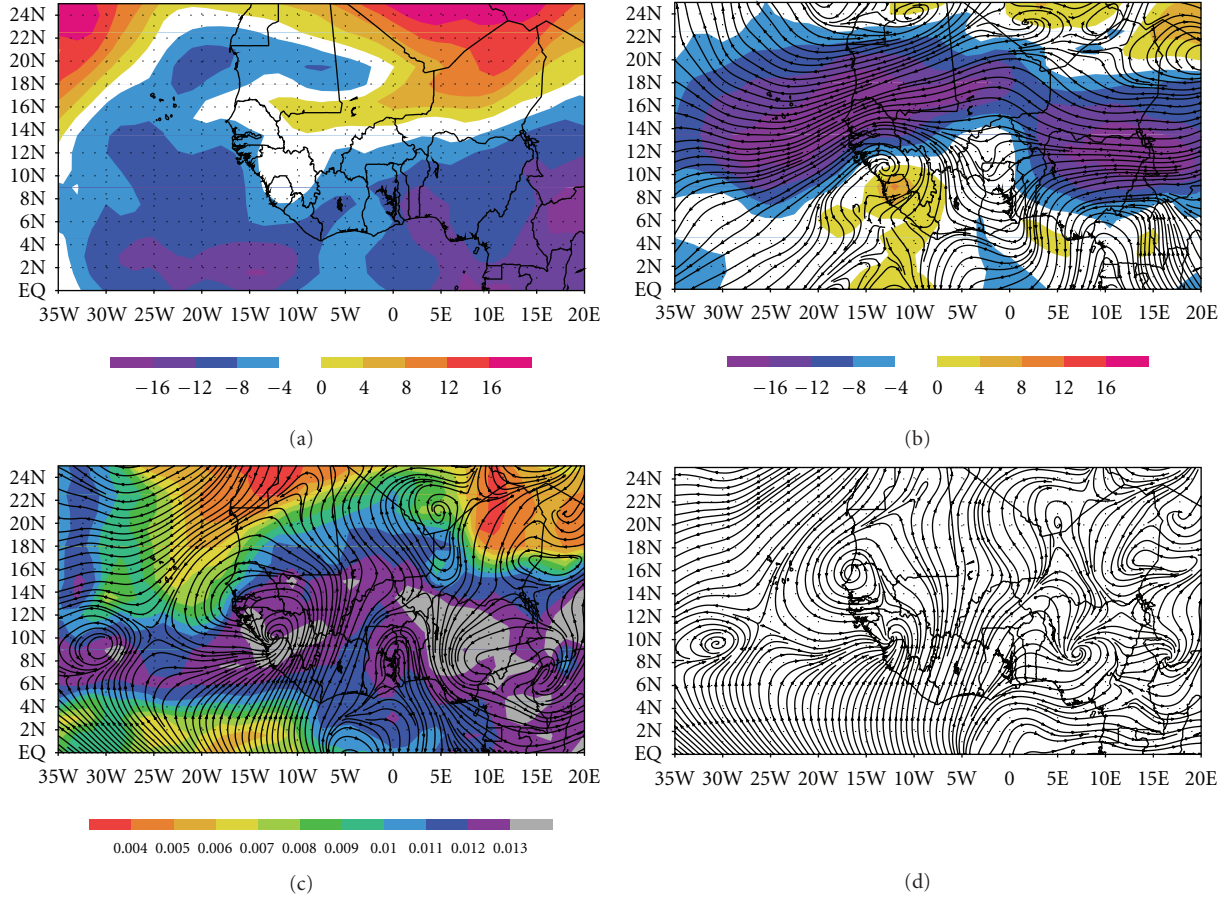


FIGURE 5: (a) ECMWF Reanalysis zonal winds ( $\text{m s}^{-1}$ ) at 1200 UTC 11 September for 200 hPa. (b) Composite ECMWF Reanalysis zonal winds ( $\text{m s}^{-1}$ ) and streamlines at 1200 UTC 11 September for 650 hPa. (c) Composite ECMWF Reanalysis specific humidity ( $\text{kg kg}^{-1}$ ) and streamlines at 1200 UTC 11 September for 850 hPa. (d) Composite ECMWF Reanalysis streamlines at 1200 UTC 11 September for 925 hPa.

TABLE 1: Depiction of the CAPE and CIN for Dakar, Kawsara, and Tambacounda, Senegal, prior to the SL propagating into the vicinity of these cities.

Locations	Time UTC	CAPE $\text{J kg}^{-1}$	CIN $\text{J kg}^{-1}$
Dakar (14.7°N, 17.5°W)	0000	3237	-269
Kawsara (14.7°N, 17.1°W)	0549	4433	-128
Tambacounda (13.8°N, 13.7°W)	0000	1112	-190

associated with the squall line passage. In Kawsara, the temperature dropped from 30.2°C at 1130 UTC to 24.8°C by 1330 UTC (Figure 7(b)). Between the hours of 0900 and 1100 UTC, the pressure rises from 1011 to 1014 hPa in Cap Skirring after the SL passage and from 1002 to 1006 hPa in Kawsara after the gust front passed. These observations are typical of squall lines and suggest a mesohigh followed the SL and gust front [7, 8]. In both locations, the pressure dropped quickly as the SL approaches and then rose afterward due to the post-SL mesohigh. Moreover, at both Kawsara and Cap Skirring, the wind shifts to an easterly direction and the speed decreases to 1.0–4.0  $\text{m s}^{-1}$  after SL passage.

3.3. *Radar and Lightning Observations.* The northern end of the heavy convection associated with the SL passes through Cap Skirring and to the south of Kawsara between 0900–1200 UTC. Surveillance reflectivity scans (Figures 8(a)–8(d)) depict heavy precipitation (reflectivity greater than 45 dBZ) propagating over Cap Skirring. By contrast, no precipitation falls over Kawsara from the squall line; nevertheless, a narrow band of relatively weak reflectivity values depict the gust front moving through this region as well. While the squall struggled to build northward, the gust front pushed as far as 50–60 km to the north and northeast of the heavier convection.

The CAPPI images in the top panels of Figures 9(a)–9(c) depict the westward progression of the SL off the coast of Senegal. The radar scans focus on the northern portion of the SL in western Senegal. These observations coupled with the surface data in Figure 7 and the surveillance scans in Figure 8 provide additional evidence that a dry gust front passes through Kawsara during the late morning of 11 September 2006.

The dashed lines on the CAPPI images are the horizontal locations of RHI cross-section plots in the bottom panels of Figures 8(a)–8(c). A reflectivity contour of 6 dBZ reaches

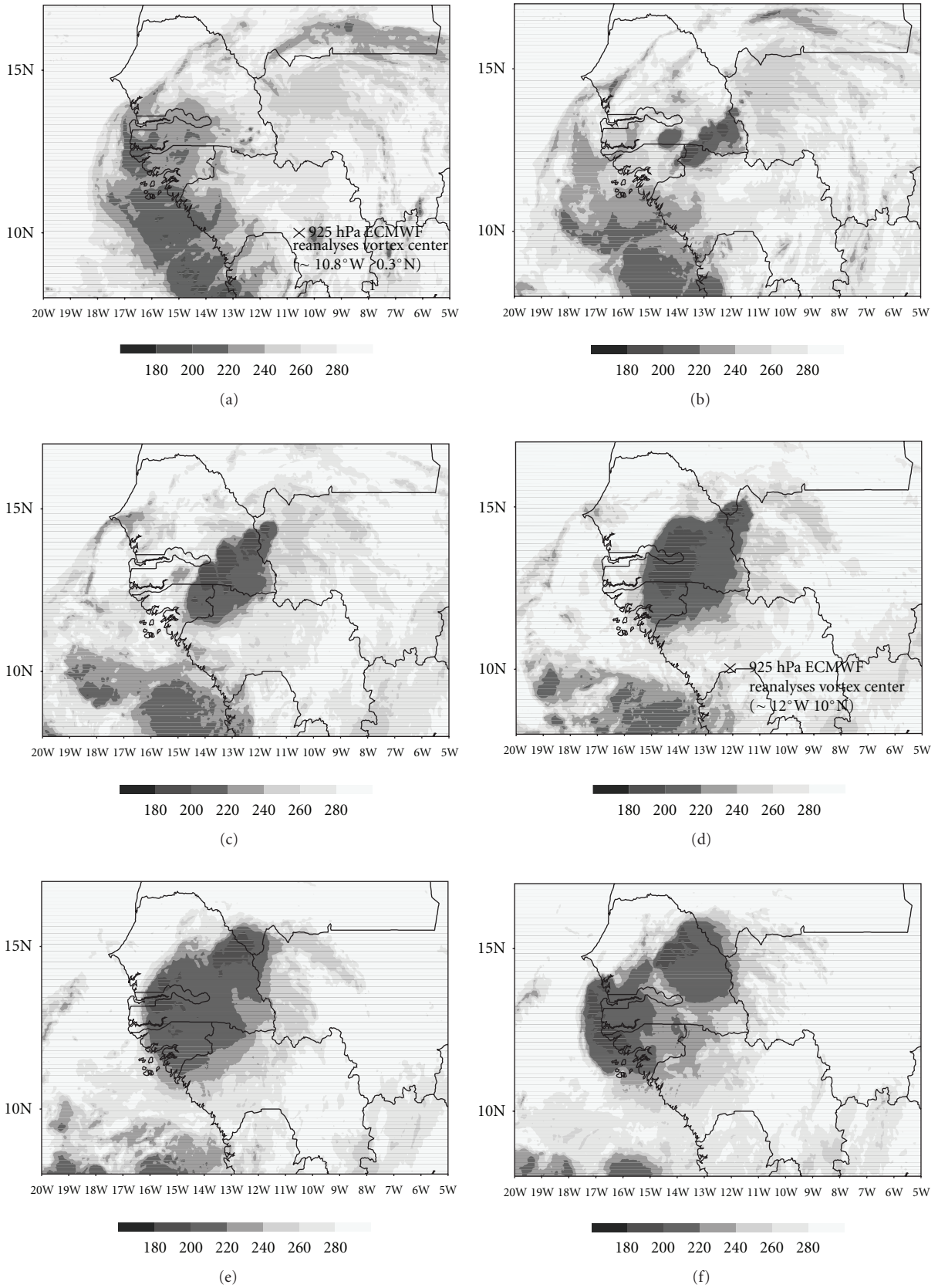


FIGURE 6: Continued.

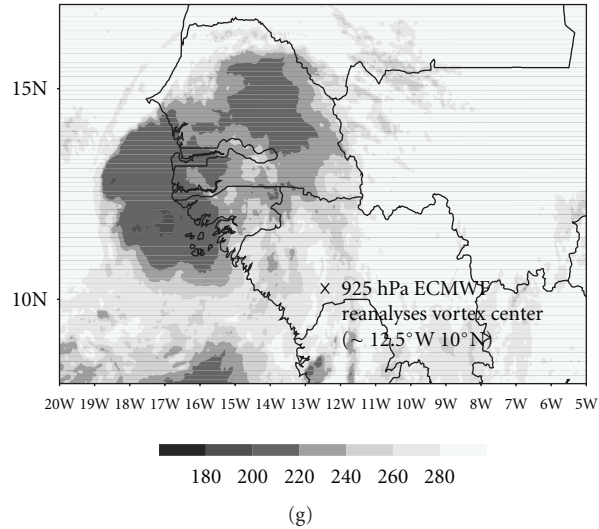


FIGURE 6: (a) Depiction of TRMM globally merged IR cloud top temperatures (K) on 11 September 2006 for 8°N to 17°N and 20°W to 5°W for 0000 UTC. The X denotes the 0000 UTC 925 hPa ECMWF Reanalyses Vortex Center. (b) Depiction of TRMM MERG IR cloud top temperatures (K) on 11 September 2006 for 8°N to 17°N and 20°W to 5°W for 0200 UTC. (c) Depiction of TRMM MERG IR cloud top temperatures (K) on 11 September 2006 for 8°N to 17°N and 20°W to 5°W for 0400 UTC. (d) Depiction of TRMM MERG IR cloud top temperatures (K) on 11 September 2006 for 8°N to 17°N and 20°W to 5°W for 0600 UTC. The X denotes the 0600 UTC 925 hPa ECMWF Reanalyses Vortex Center. (e) Depiction of TRMM globally merged IR cloud top temperatures (K) on 11 September 2006 for 8°N to 17°N and 20°W to 5°W for 0800 UTC. (f) Depiction of TRMM MERG IR cloud top temperatures (K) on 11 September 2006 for 8°N to 17°N and 20°W to 5°W for 1000 UTC. (g) Depiction of TRMM MERG IR cloud top temperatures (K) on 11 September 2006 for 8°N to 17°N and 20°W to 5°W for 1200 UTC. The X denotes the 1200 UTC 925 hPa ECMWF Reanalyses Vortex Center.

up to nearly 15 km AGL, which is consistent with higher cloud top heights at 0900 UTC (see Figure 6). However, while the 48 dBZ contour extends horizontally for 10 km, it only reached an altitude of 3 km AGL. This horizontally extensive but shallow convection is consistent with the general lack of convective intensity seen in this SL at 0900 UTC. At this time, there is no trailing stratiform rain region associated with this SL. Surveillance scans to the south (see Figure 8) further reveal this underdeveloped stratiform region.

As the squall line transitions from a continental to maritime regime, the convection associated with it became shallower and less intense (Figure 9(b)). The reduced amount of CAPE offshore relative to land most likely contributed to the decrease in convective intensity; dropsondes released offshore on 12 September indicated maximum CAPE values of approximately  $2500 \text{ J kg}^{-1}$  (not shown), considerably less than the values observed over land the previous day. A study investigating an mesoscale convective system moving over West Africa on 31 August 2006 also noted less favorable thermodynamic and dynamic conditions offshore that contributed to convective weakening [19]. Although there were a few small cells with 54 dBZ contours at 4 km AGL observed in the horizontal cross section, the vertical cross section taken through the leading edge shows the 42 dBZ contour reaching only slightly above 4 km AGL. A secondary reflectivity maximum at approximately 47 to 50 km distance along the dashed line cross section is also observed. This suggests that decaying cells from the convective leading edge move rearward once they have reached a mature stage [20]. However, at 1000 UTC (Figure 9), the stratiform rain region

is even less cohesive with the leading edge to the west than it was at 0900 UTC. This lack of cohesion of the stratiform region is uncharacteristic of SLs observed in GATE and COPT 81 [3, 5–8]. Figure 9(c) shows that the northern end of the SL is approximately 50 km southwest of the NPOL radar location at 1100 UTC.

Figure 10 depicts the UK-ATD lightning data [21, 22] between 0400–1200 UTC on 11 September 2006. Lightning flashes show that the SL extended southward from approximately 14.5°N to 12.5°N from 0400 to 0600 UTC as shown by purple crosses. Lightning associated with the SL moved westward from 0600 to 0800 UTC as shown by blue circles. Between 0800–1000 UTC, the lightning flashes associated with the SL as shown by red squares approached the West African coastline. The lightning flashes associated with the SL moved westward into the Atlantic between 1000–1200 UTC shown by the yellow triangles. The region of lightning flashes to the northeast of the SL persisted throughout this time period.

#### 4. Observations of Saharan Air Layer Outbreak

A significant SAL outbreak, one of five observed between 15 August and 15 September 2006 [23], preceded the SL on 11 September 2006. SAL outbreaks are defined as the onset of a well-mixed, warm, dry, and dusty air mass 2.0 to 6.0 km deep that originates from Saharan Africa and propagates westward toward the Eastern Atlantic Ocean [24]. This air mass (bounded by temperature inversions at its base and top)



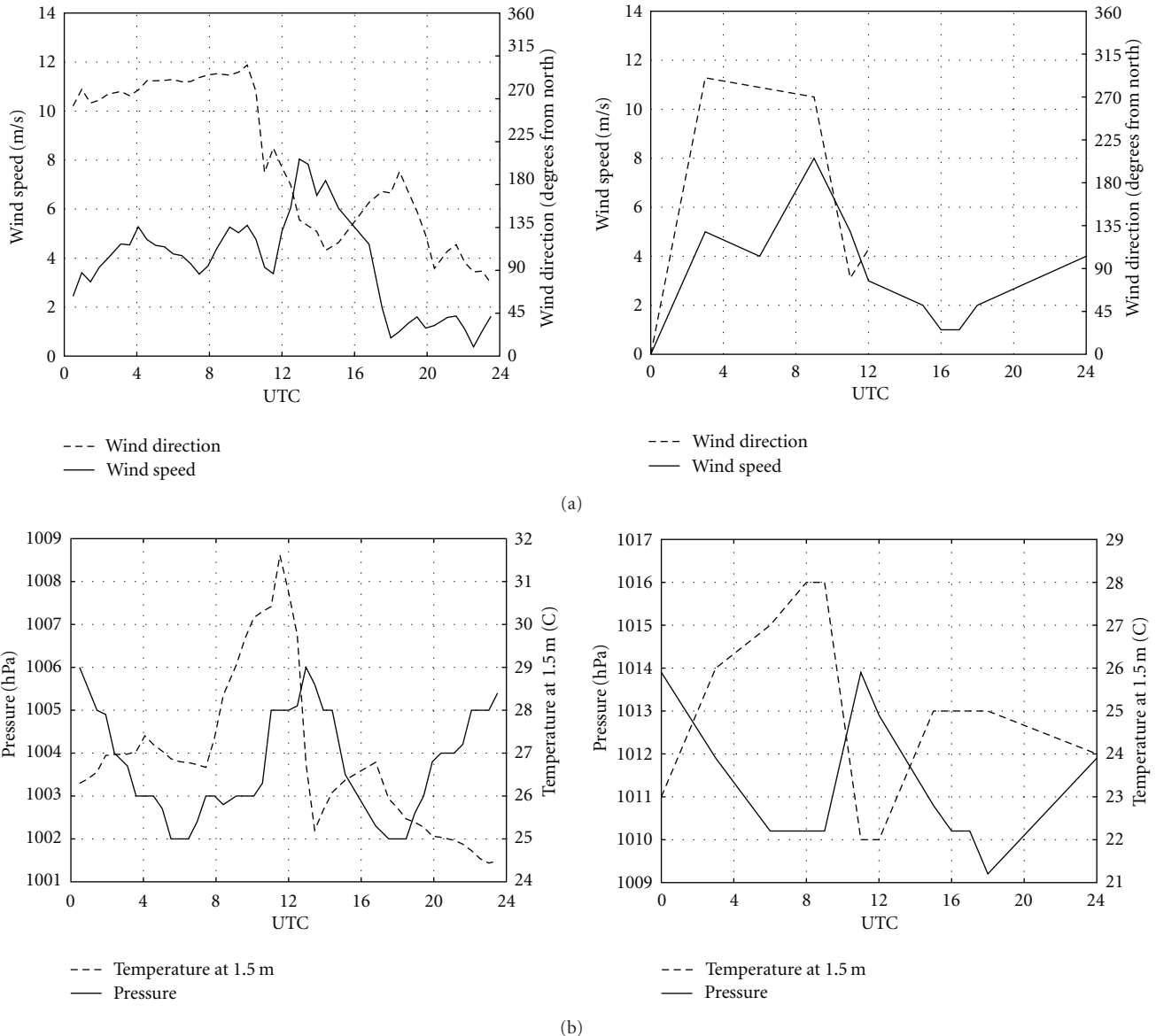


FIGURE 7: (a) Double  $y$ -axis plots containing an 11 September 2006 time series of wind speed in  $\text{m s}^{-1}$  and wind direction in degrees from north for Kawsara and Cap Skirring, Senegal. (b) Double  $y$ -axis plots containing an 11 September 2006 time series of pressure in hPa denoted by the solid line and 1.5 m temperature in  $^{\circ}\text{C}$  denoted by the dashed line.

is usually 5 to 6 $^{\circ}\text{C}$  warmer than the more humid and shallow (e.g., 1.2 to 1.8 km) marine boundary layer air below [25–27]. Typically the AEJ forms around 650 hPa on the southern edge of the SAL primarily due to the temperature contrast between the warm SAL to the north and the relatively cooler marine air to its south [24, 28, 29].

The ECMWF Reanalyses of 850 hPa specific humidity on 11 September (see Figures 3(c), 4(b), and 5(c)) indicate a tongue of low specific humidity (values less than  $0.009 \text{ kg kg}^{-1}$ ) extending south into coastal and northern Senegal. The low moisture measurements are indicative of drier air and dust intruding from the Saharan Desert into northern Senegal. The moisture steadily increases to the

south and east over southeast Senegal, Mali, and Guinea-Bissau.

Rawinsonde data also show the presence of the SAL in the vicinity of the SL on 11 September 2006. At 0000 UTC, the SAL (though weak and shallow) is present at Tambacounda, Senegal (Figure 11(a)) and (more prominently) in Dakar (Figure 11(b)) and at 0549 UTC in Kawsara (Figure 11(c)). The depth of the SAL is denoted by the vertical extent of the SAL between its lower and upper temperature inversions. At Dakar (Figure 11(b)), the SAL extends from 935 hPa to 580 hPa, while at Kawsara (Figure 9(c)) it starts at 900 hPa and is capped at 600 hPa. At both locations (Figures 11(b) and 11(c)), there is a robust dewpoint depression on

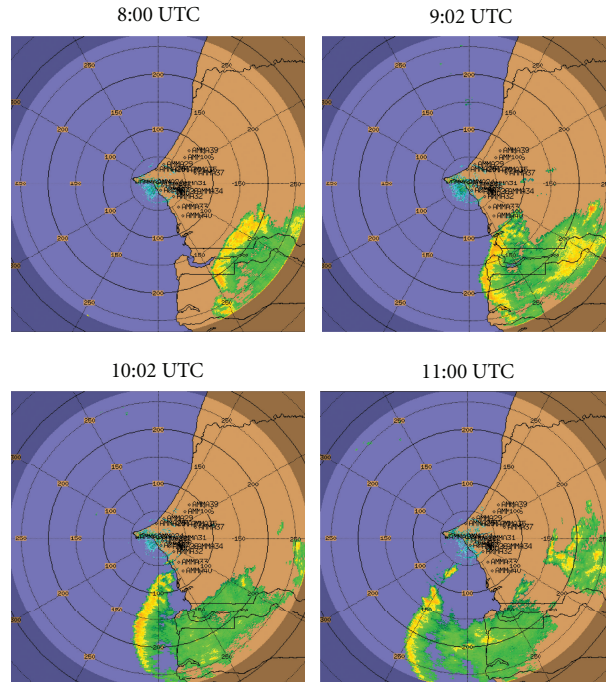


FIGURE 8: Surveillance scans of radar reflectivity (dBZ) time series for 0800 UTC, 0902 UTC, 1002 UTC, and 1100 UTC on 11 September 2006. The black circles designate the 100, 150, 200, and 250 km radial distances from the NPOL radar.

the order of 15 to 20°C in the layer of 850 to 800 hPa. The depth and atmospheric stability of the SAL in Dakar and Kawsara prevented the squall line from building this far north. At the same time, the rather weak and shallow SAL at Tambacounda did not impede the squall line here.

Post-SL rawinsonde (Figure 12(a)) data indicate a moist profile (modified by the squall line passage just before 0800 UTC) at 1200 UTC for Tambacounda. At both Dakar (1200 UTC, Figure 12(b)) and Kawsara (1402 UTC, Figure 12(c)), a deep SAL layer remains after the squall has moved to the west of this region. The SAL exists between 920 hPa and 610 hPa at Dakar. The highest dewpoint depression at Dakar and Kawsara (Figure 12(c)) is around 875 hPa where the dewpoint was 7°C while the temperature is 26°C.

At Mbour (see location in Figure 1), Figures 13(a)–13(d) depict aerosol optical thickness (AOT) measurements from the Aerosol Robotic Network (AERONET) Dakar station. Low AOT values below 0.30 are found on 08 September (Figure 13(a)), and a steady increase is observed over subsequent days (Figures 13(b)–13(d)). By 10 September (Figure 13(c)), AOT values are approximately 0.65 and increase to 0.71 during the early morning of 11 September. The high AOT values on 10–11 September are indicative of the dustiness associated with the SAL. The AOT values, in concert with the wind flow at 925 hPa and 850 hPa, suggest that the dry, dusty SAL is being entrained into the squall line inflow.

Two-day back-trajectories from the HYSPLIT Model at Dakar, Kawsara, and Tambacounda (Figure 14) illustrate the origins of the air mass at various altitudes over western Senegal on 11 September. The air mass at 3.0 km in altitude

in Tambacounda at 1200 UTC 10 September originated out of the Sahara; by contrast, the origin of the air mass at 0.5 km and 1.5 km originates over the Eastern Atlantic basin and northern Senegal, respectively (Figure 14(a)). Dakar and Kawsara exhibit airflow from the Sahara at both 1.5 km and 3.0 km at 0000 UTC 11 September (Figure 14). This deeper airflow out of the Sahara explains the greater vertical extent of the SAL and stronger temperature inversion at its base over Dakar and Kawsara as compared to Tambacounda. These conditions also contributed to enhanced atmospheric stability, which lead to weakening of the northern portion of the squall line.

## 5. Discussion

The SL was generated by an AEW in southeastern Senegal at 0000 UTC on 11 September 2006 (Figure 6). A SAL outbreak was building into the western Senegal and the adjacent Atlantic Ocean waters. The SL approached the coast and was several hundred kilometers ahead of the AEW vortex by 0900 UTC. The southern two-thirds of the SL maintained its strength. This is noted by its NPOL reflectivity and the robust lightning flashes observed by WWLLN south of 14°N. The northern third weakened in the presence of abundant dust noted by the lack of lightning north of 14°N (Figure 10), the Kawsara and Dakar radiosondes (Figures 11(a) and 11(b), 12(a) and 12(b)), increasingly high AOT at Mbour (Figure 13), no recorded rainfall by the AMMA22 and AMMA23 rain gauges (not shown), and precipitation-free boundary in Kawsara during the 0900 to 1200 UTC hour. Moreover, HYSPLIT modeling (Figure 14) provides

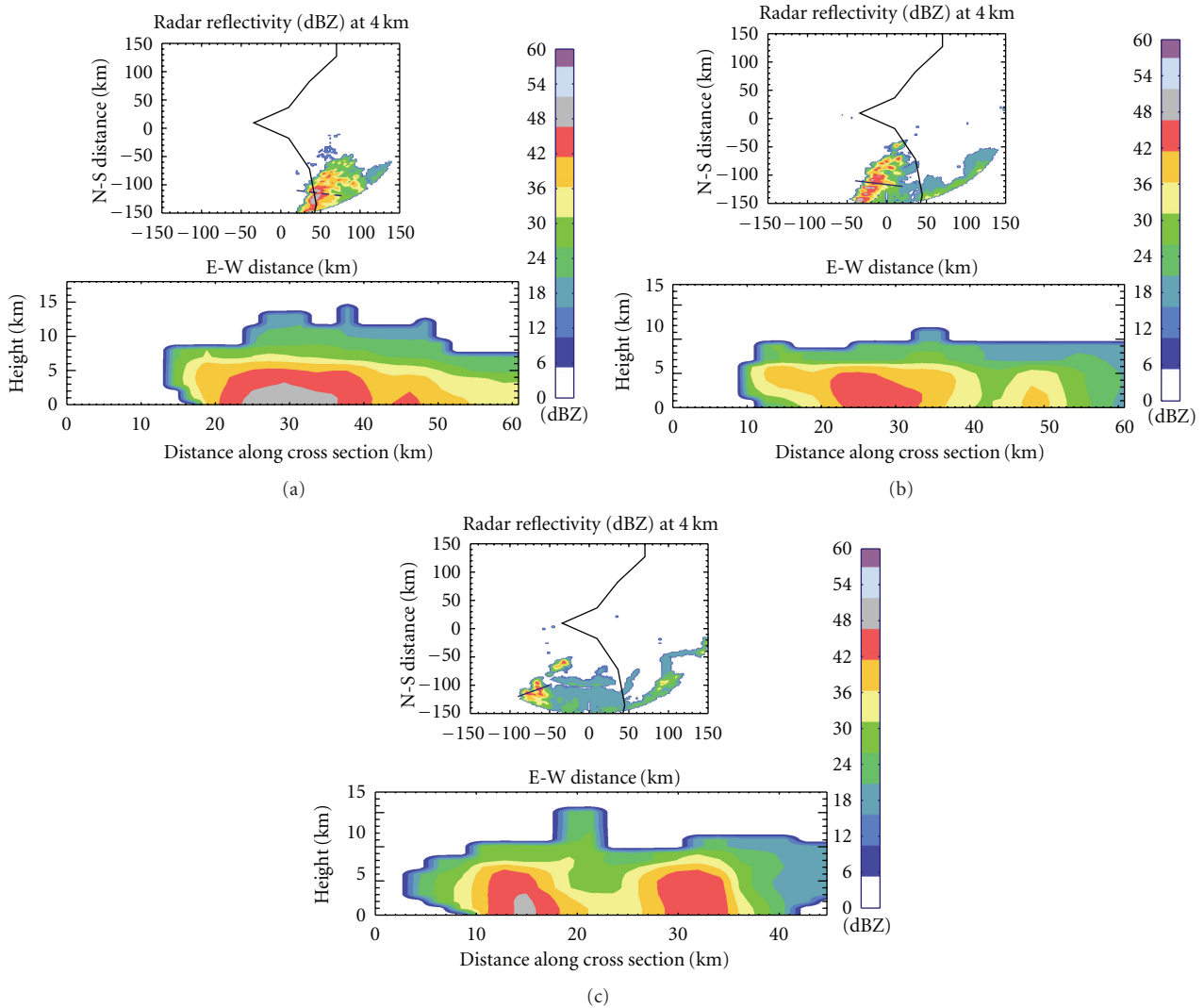


FIGURE 9: (a) A horizontal constant altitude plan position indicator (CAPPI) image at 4.0 km altitude and radar height indicator RHI plots of the NPOL radar reflectivity (dBZ) along the leading convective line on 11 September 2006 at 0900 UTC. The negative sign in the CAPPI images indicates distance in the westward direction. The dashed line in the CAPPI image represents the location of the cross section. In the RHI images, ordinate axis is height  $z$  in km and the azimuthal is the distance in km along the cross-section. (b) A horizontal constant altitude plan position indicator (CAPPI) image at 4.0 km altitude and radar height indicator RHI plots of the NPOL radar reflectivity (dBZ) along the leading convective line on 11 September 2006 at 1000 UTC. The negative sign in the CAPPI images indicates distance in the westward direction. The dashed line in the CAPPI image represents the location of the cross section. In the RHI images, ordinate axis is height  $z$  in km and the azimuthal is the distance in km along the cross-section. (c) A horizontal constant altitude plan position indicator (CAPPI) image at 4.0 km altitude and radar height indicator RHI plots of the NPOL radar reflectivity (dBZ) along the leading convective line on 11 September 2006 at 1100 UTC. The negative sign in the CAPPI images indicates distance in the westward direction. The dashed line in the CAPPI image represents the location of the cross section. In the RHI images, ordinate axis is height  $z$  in km and the azimuthal is the distance in km along the cross-section.

evidence that particles in coastal Senegal at 0800 to 1000 UTC originated from the Sahara implying that Saharan dust was present in this region.

The reflectivity values in Figure 8 indicate that the southern part of the SL weakened as it propagated off the coast, particularly by 1100 UTC; however, the reflectivity is the only observation that reveals the southern portion of the SL weakens. This is similar to the transition the 31 August SL in DeLonge et al. [19]. No solid conclusion can be

made on the SL and AEW transition to Hurricane Helene. There are not aircraft observations or TRMM overpasses over this SL on 11 September to make the connection. More aircraft- and surface-based measurements are needed to tie this AEW and SL to other coastally transitioning storms. The next set of aircraft observations are not until 12 September 2006. At this time, the AEW develops into Hurricane Helene by then (Jenkins et al. [23] and Zawislak and Zipser [15]).



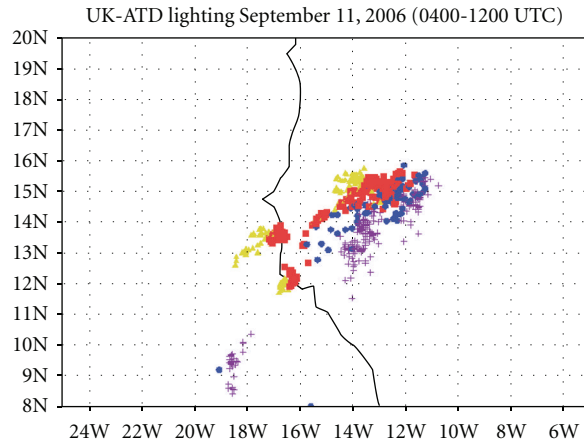


FIGURE 10: An image of cloud-to-ground lightning flashes on 11 September 2006 between 0400 and 1200 UTC. Purple crosses are for CG flashes from 0400 to 0600 UTC; blue circles are for flashes from 0600 to 0800 UTC; red squares are for flashes from 0800 to 1000 UTC; yellow triangles are for flashes from 1000 to 1200 UTC.

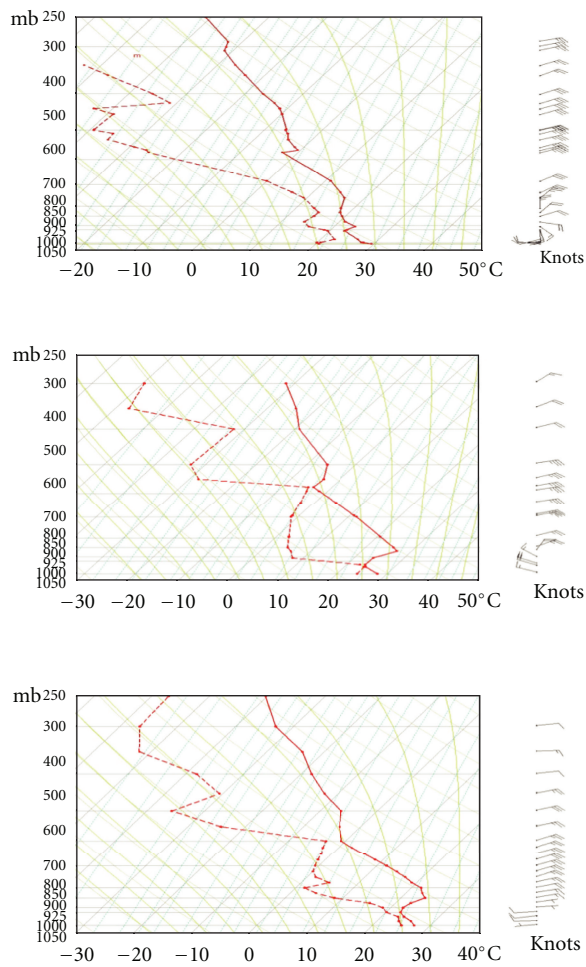


FIGURE 11: Rawinsonde of temperature and dewpoint and wind profiles (kts) for Tambacounda at 1200 UTC on 10 September, Dakar at 0000 UTC on 11 September, and Kawsara at 0530 UTC on 11 September 2006. The solid line is temperature, the dashed line is dewpoint, and both are given in degrees C. The soundings are plotted every 50 hPa.

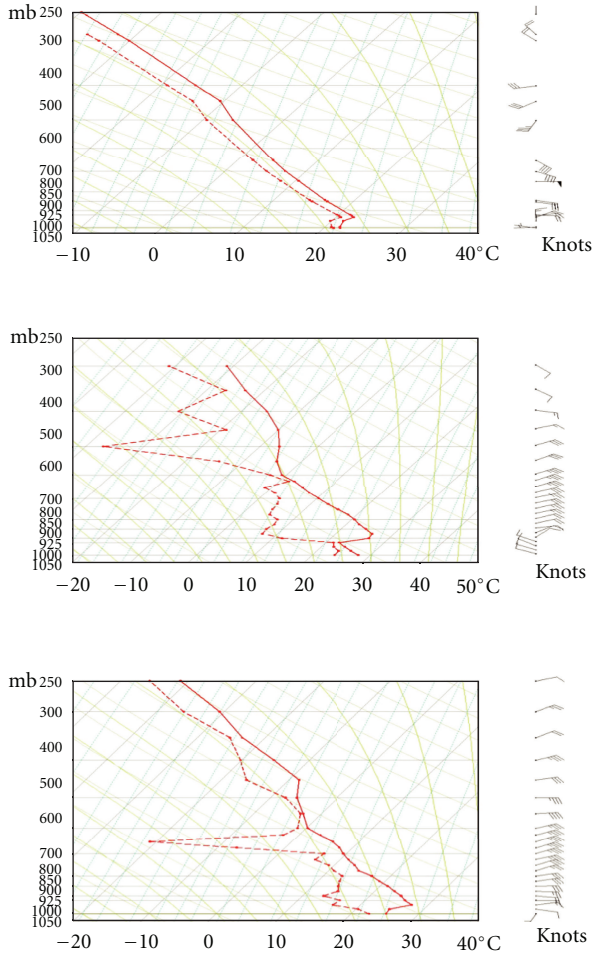


FIGURE 12: Same as Figure 9 but at Tambacounda at 1200 UTC, Dakar at 1200 UTC, and Kawsara at 1402 UTC on 11 September 2006.

## 6. Conclusion

The NAMMA-06 campaign provided measurements for coastal Senegal. These observations provided insight into the dynamics and thermodynamics of the SL and SAL. The ECMWF Reanalyses show that the AEW and SL were in a favorable environment for continued strengthening and maturing. These observations included ground-based measurements such as flux tower measurements, radiosonde launches, and AERONET. There was remote sensing data from the NPOL radar, TRMM MERG, and MODIS satellite products. These observations revealed that the westerly propagating SL and the SAL in the lower troposphere interacted. The interaction was evident through the weakening of the northern portion of the SL. The HYSPLIT back-trajectory model gives indication of impending dust. Even though CAPE was high and an SL-related boundary passed through Kawsara, there was not precipitation on its northern end.

There are avenues for additional work on this paper. Additional plausible ideas for future research include aircraft observations that might identify the role SAL aerosols have

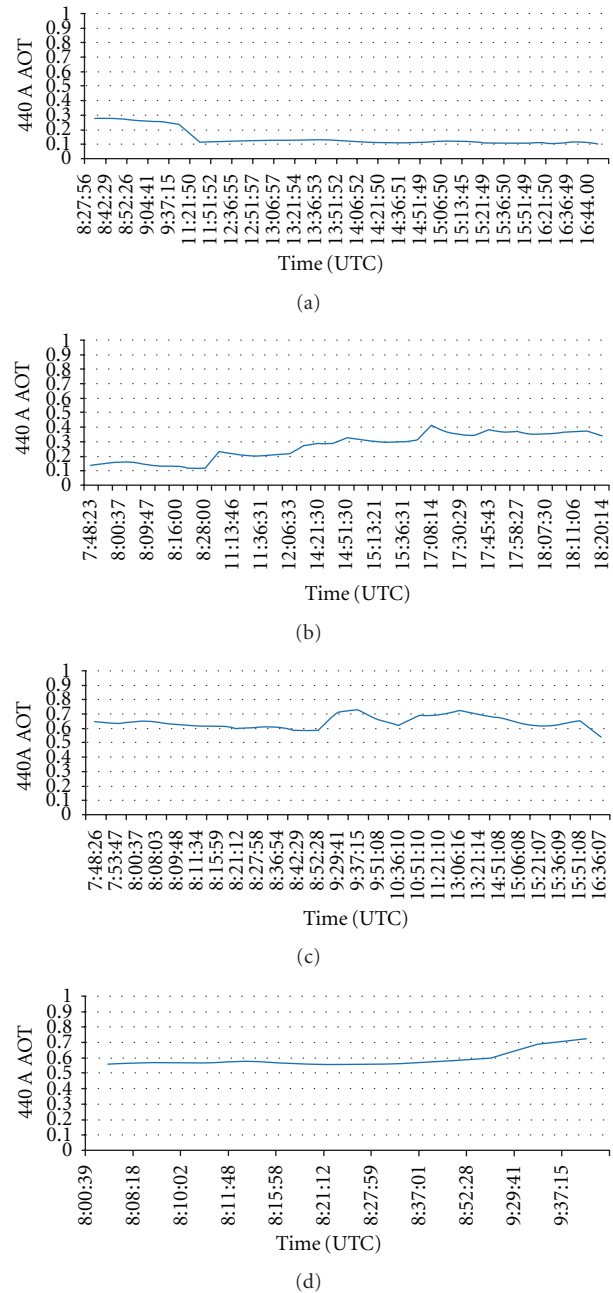


FIGURE 13: (a) A time series plot of 440 Angstrom AOT for 8 September 2006 at Mbour, Senegal. (b) A time series plot of 440 Angstrom AOT for 9 September 2006 at Mbour, Senegal. (c) A time series plot of 440 Angstrom AOT for 10 September 2006 at Mbour, Senegal. (d) A time series plot of 440 Angstrom AOT for 11 September 2006 at Mbour, Senegal.

on clouds, precipitation, and developing tropical systems. Despite there being observations and arguments to support the negative interaction of the two (e.g., Wong and Dessler [30]), there is evidence that dust and aerosol entrainment into convective systems acts as cloud condensation nuclei subsequently forming precipitation and banding. Wong and Dessler [31] concluded that Saharan dust increased the number of cumulus cloud particles in the North Atlantic

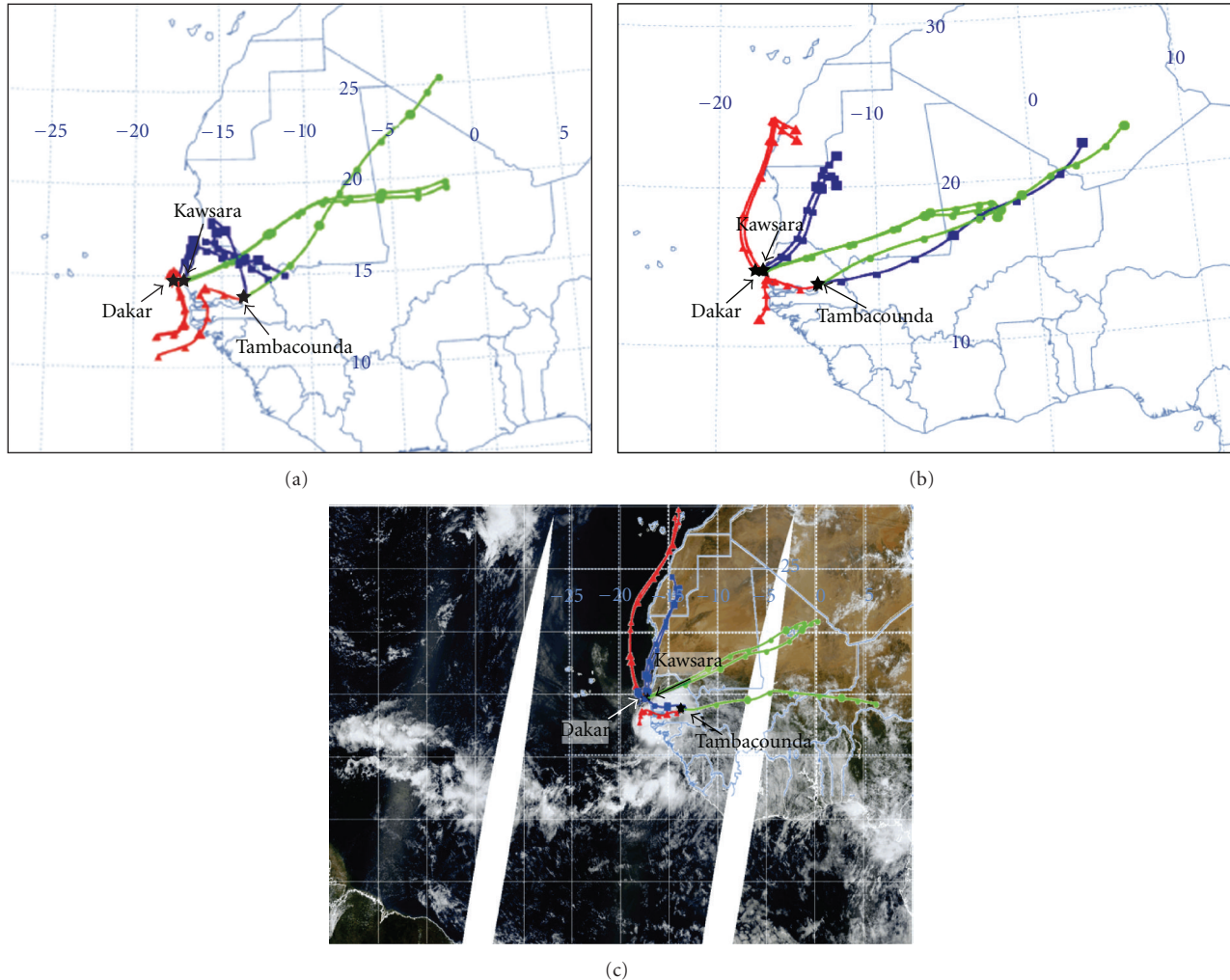


FIGURE 14: (a) The 48-hour HYSPLIT back-trajectory valid for 1200 UTC 10 September 2006. (b) The 48-hour HYSPLIT back-trajectory valid for 0000 UTC 11 September 2006. (c) The 1150 UTC Terra MODIS Visible Composite Satellite and 48-hour HYSPLIT back-trajectories valid 1200 UTC, 11 September 2006. Back-trajectories are for air parcels at 0.5 km AGL (red), 1.5 km AGL (blue), and 3.0 km AGL (green).

in the summer of 2006. Rainbands of 2006 Tropical Storm Debby were invigorated by dust (Jenkins et al. [23]). The precipitation-free gust front that passed through Kawsara is an interesting phenomena to explore.

Exploring these topics include high-resolution mesoscale model simulations of AEWs, SLs, and SAL outbreaks, which combine cloud microphysics, aerosols, and precipitation. Sensitivity tests of microphysical, convective, planetary boundary layer, and aerosol schemes could be done for the Western and Central African continent and the Eastern Atlantic Ocean. Answers to these questions would provide rich insight into SL, AEW, and SAL formation, characteristics, and interactions and to how crucial they are to forecasting in the Eastern Tropical Atlantic Ocean.

## Acknowledgments

The authors thank G. S. Jenkins, Ph. D., Professor in the Howard University Department of Physics and Astronomy

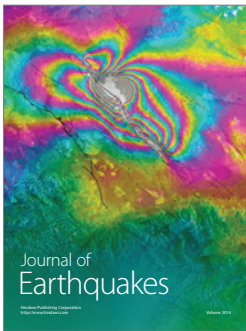
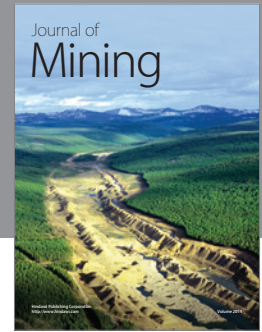
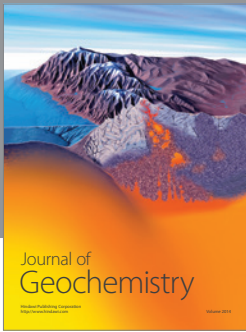
and the Program in Atmospheric Sciences for constructive dialogue and suggestions on this paper. They thank B. Emory of Goddard Space Flight Center for his critique of the text. The Dakar AERONET data was provided by D. Tanre. This study was funded by National Science Foundation (NSF) Grant OISE-0553959 and NASA Grant no. NNX06AC78G.

## References

- [1] S. W. Payne and M. M. McGarry, "The relationship of satellite inferred convective activity to easterly waves over West Africa and the adjacent ocean during phase III of GATE," *Monthly Weather Review*, vol. 105, pp. 413–420, 1977.
- [2] A. Gaye, A. Viltard, and P. de Félice, "Squall lines and rainfall over Western Africa during summer 1986 and 87," *Meteorology and Atmospheric Physics*, vol. 90, no. 3-4, pp. 215–224, 2005.
- [3] R. A. Houze, "Structure and dynamics of a tropical squall line system," *Structure and Dynamics of a Tropical Squall Line System*, vol. 105, pp. 1540–1567, 1977.



- [4] C. Thorncroft and K. Hodges, "African easterly wave variability and its relationship to Atlantic tropical cyclone activity," *Journal of Climate*, vol. 14, no. 6, pp. 1166–1179, 2001.
- [5] D. P. Rowell and J. R. Milford, "On the generation of African squall lines," *Journal of Climate*, vol. 6, no. 6, pp. 1181–1193, 1993.
- [6] E. J. Zipser, "Mesoscale and convective-scale downdrafts as distinct components of SL circulation," *Monthly Weather Review*, vol. 105, pp. 1568–1589, 1977.
- [7] M. Chong, P. Amayenc, G. Scialom, and J. Testud, "A tropical squall line observed during the COPT 81 experiment in West Africa: part 1: kinematic structure inferred from dual-Doppler radar data," *Monthly Weather Review*, vol. 115, no. 3, pp. 670–694, 1987.
- [8] J. P. Chalon, G. Jaubert, F. Roux, and J. P. Lafore, "The West African squall line observed on 23 June 1981 during COPT 81: mesoscale structure and transports," *Journal of the Atmospheric Sciences*, vol. 45, no. 19, pp. 2744–2763, 1988.
- [9] F. Roux, "The West African squall line observed of 23 June 1981 during COPT 81: kinematics and thermodynamics of the convective region," *Journal of the Atmospheric Sciences*, vol. 45, no. 3, pp. 406–426, 1988.
- [10] J. Schwendike and S. C. Jones, "Convection in an African easterly wave over West Africa and the eastern Atlantic: a model case study of Helene (2006)," *Quarterly Journal of the Royal Meteorological Society*, vol. 136, no. 1, pp. 364–396, 2010.
- [11] T. N. Carlson, "Synoptic histories of three African disturbances the developed into Atlantic hurricanes," *Monthly Weather Review*, vol. 97, pp. 256–276, 1969.
- [12] T. N. Carlson, "Some remarks on African disturbances and their progress over the tropical Atlantic," *Monthly Weather Review*, vol. 97, pp. 716–726, 1969.
- [13] R. W. Burpee, "The origin and structure of easterly waves in the lower troposphere of North Africa," *Journal of the Atmospheric Sciences*, vol. 29, 1972.
- [14] R. J. Reed, D. C. Norquist, and E. E. Recker, "The structure and properties of African wave disturbances as observed during Phase III of GATE," *Monthly Weather Review*, vol. 105, pp. 317–333, 1977.
- [15] J. Zawislak and E. J. Zipser, "Observations of seven African easterly waves in the east Atlantic during 2006," *Journal of the Atmospheric Sciences*, vol. 67, no. 1, pp. 26–43, 2010.
- [16] E. J. Zipser, C. H. Twohy, S.-C. Tsay et al., "The Saharan air layer and the fate of African Easterly Waves: NASA's AMMA 2006 field program to study tropical cyclogenesis: NAMMA," *Bulletin of the American Meteorological Society*, vol. 8, pp. 1137–1156, 2009.
- [17] P. Kållberg, A. Simmons, S. Uppala, and M. Fuentes, "The ERA-40 archive," Tech. Rep., ECMWF, 2007, [http://www.ecmwf.int/publications/library/ecpublications/\\_pdf/era40/ERA40\\_PRS17\\_rev1.pdf](http://www.ecmwf.int/publications/library/ecpublications/_pdf/era40/ERA40_PRS17_rev1.pdf).
- [18] J. E. Janowiak, R. J. Joyce, and Y. Yarosh, "A real-time global half-hourly pixel-resolution infrared dataset and its applications," *Bulletin of the American Meteorological Society*, vol. 82, no. 2, pp. 205–217, 2001.
- [19] M. S. DeLonge, J. D. Fuentes, S. Chan et al., "Attributes of mesoscale convective systems at the land-ocean transition in Senegal during NASA African Monsoon Multidisciplinary Analyses 2006," *Journal of Geophysical Research D*, vol. 115, no. 10, Article ID D10213, 2010.
- [20] R. A. Houze, S. A. Rutledge, M. I. Biggerstaff, and B. F. Smull, "Interpretation of Doppler weather radar displays of mid-latitude mesoscale convective systems," *Bulletin—American Meteorological Society*, vol. 70, no. 6, pp. 608–619, 1989.
- [21] J. Nash, "Progress in introducing new technology sites for the Met Office long range lightning detection system," Tech. Rep. 2.9, Paper 2.9 WMO, WMO/TD-No.1265.
- [22] S. Keogh, E. Hibbett, J. Nash, and J. Eyre, "The Met Office Arrival Time Difference (ATD) system for thunderstorm detection and lightning location," Tech. Rep. 488, Met Office, Numerical Weather Prediction: Forecasting Research, 2006.
- [23] G. Jenkins, P. Kucera, E. Joseph et al., "Coastal observations of weather features in Senegal during the African monsoon multidisciplinary analysis special observing period 3," *Journal of Geophysical Research D*, vol. 115, no. 18, Article ID D18108, 2010.
- [24] V. M. Karyampudi and T. N. Carlson, "Analysis and numerical simulations of the Saharan air layer and its effect on easterly wave disturbances," *Journal of the Atmospheric Sciences*, vol. 45, no. 21, pp. 3102–3136, 1988.
- [25] B. Marticorena and G. Bergametti, "Two-year simulations of seasonal and interannual changes of the Saharan dust emissions," *Geophysical Research Letters*, vol. 23, no. 15, pp. 1921–1924, 1996.
- [26] I. Koren and Y. J. Kaufman, "Direct wind measurements of Saharan dust events from Terra and Aqua satellites," *Geophysical Research Letters*, vol. 31, no. 6, pp. L06122–4, 2004.
- [27] C. H. Twohy, S. M. Kreidenweis, T. Eidhammer et al., "Saharan dust particles nucleate droplets in eastern Atlantic clouds," *Geophysical Research Letters*, vol. 36, no. 1, Article ID L01807, 2009.
- [28] T. N. Carlson and J. M. Prospero, "The large-scale movement of Saharan air outbreaks over Northern Equatorial Atlantic," *Journal of Applied Meteorology*, vol. 11, pp. 283–297, 1972.
- [29] J. P. Dunion and C. S. Velden, "The impact of the Saharan Air Layer on Atlantic tropical cyclone activity," *Bulletin of the American Meteorological Society*, vol. 85, no. 3, Article ID L12804, pp. 353–365, 2004.
- [30] G. S. Jenkins and A. Pratt, "Saharan dust, lightning and tropical cyclones in the eastern tropical Atlantic during NAMMA-06," *Geophysical Research Letters*, vol. 35, no. 12, Article ID L12804, 2008.
- [31] S. Wong and A. E. Dessler, "Suppression of deep convection over the tropical North Atlantic by the Saharan Air Layer," *Geophysical Research Letters*, vol. 32, no. 9, Article ID L09808, 4 pages, 2005.



**Hindawi**

Submit your manuscripts at  
<http://www.hindawi.com>

